Yang, Tingqiang ; Hemeryck, Anne ; Pokhrel, Suman ; Chen, Wen ; Mädler, Lutz ; Weimar, Udo ; Barsan, Nicolae

HCHO Sensing Mechanism of In4Sn3O12 Revealed by DRIFTS and DFT

Journal Article as: peer-reviewed accepted version (Postprint)

DOI of this document*(secondary publication): https://doi.org/10.26092/elib/3704

Publication date of this document: 19/02/2025

* for better findability or for reliable citation

HCHO Sensing Mechanism of $In_4Sn_3O_{12}$ Revealed by DRIFTS and DFT

Tingqiang Yang,[1,2] Anne Hemeryck,[2,*] Suman Pokhrel,[3] Wen Chen,[4] Lutz Mädler,[3] Udo Weimar,[1] Nicolae Barsan[1,*]

[1] Institute of Physical and Theoretical Chemistry and Center for Light-Matter Interaction, Sensors & Analytics (LISA+), University of Tübingen, D-72076 Tübingen, Germany

[2] LAAS-CNRS, Université de Toulouse, CNRS, Toulouse, France

[3] Foundation Institute of Materials Science (IWT), Department of Production Engineering, University of Bremen, Bremen, Germany

[4] State Key Laboratory of Silicate Materials for Architectures, School of Materials Science and Engineering, Wuhan University of Technology, 430070 Wuhan, China

*Corresponding authors:

Nicolae Barsan: nb@ipc.uni-tuebingen.de

Anne Hemeryck: anne.hemeryck@laas.fr

Abstract

The combination of operando DRIFTS measurement and DFT calculation reveals the counterintuitive HCHO sensing mechanism of $In_4Sn_3O_{12}$. We identified the partial oxidation of HCHO into formate (or HCOOH), a process with medium activation energy (0.43−0.68 eV) and sufficient electron donation effect, as responsible for the sensor signal at the optimum temperature of 200 ℃. The Sn (3a)-connected O is the active site and plays key roles in both HCHO adsorption and partial oxidation.

Formaldehyde (HCHO), a harmful indoor air pollutant normally emitted from building materials and some household furniture, is a very significant nuisance.[1] Distributed HCHO monitoring is very necessary and this would require high performance, low cost and low power sensors. Gas sensors based on semiconducting metal oxides (SMOX) could be a solution, if sufficiently selective, because of their success in various applications where low cost and power was required.[2]

$In_4Sn_3O_{12}$ nanoparticles was previously identified as a promising HCHO sensing material because of the ultrahigh sensor signal as well as good selectivity.[3] However, the reasons of that behavior were not clarified. The commonly accepted sensing mechanism of volatile organic compounds (VOCs) – namely complete oxidation into CO_2 and H_2O by surface oxygen species and in the process electrons that were involved in the bonding of the surface oxygen species donated to the semiconductor[4] – could be oversimplified and has huge difficulty in explaining selectivity of $In_4Sn_3O_{12}$ to HCHO against the other VOCs. A thorough explanation for the excellent HCHO sensitivity and selectivity of $In_4Sn_3O_{12}$ is not only a very interesting scientific question but, because its understanding could open new avenues for gas sensing and HCHO oxidation removal by SMOX,[5, 6, 7] also having a practical relevance.

Herein, HCHO sensing mechanism of $In_4Sn_3O_{12}$ is going to be revealed. Encouraged by the success of the combination between in operando Diffuse Reflectance Infrared Fourier Transform Spectroscopy (DRIFTS) with Density Functional Theory (DFT) calculations,[8] we applied the same approach.

The DRIFTS is measured at optimum temperature (200 °C) in dry condition; the exposure is at ppm levels. The recorded sensor signals are high (Figure 1a), and the DRIFTS absorbance spectra show the formation of various surface species except the combustion products of CO_2 or CO, which somehow overthrows the generally accepted sensing mechanism. One can clearly identify formate species (Figure 1b), whose asymmetric vibration ($\nu_{as}COO^-$) frequency sits around 1576 cm^{-1} and symmetric vibration (ν_sCOO^-) frequency splits at 1381 and 1354 cm^{-1} due to interaction with CH.[6, 9] The weak peaks at 2968 and 2887 cm^{-1} are attributed to $\nu_{as}CH_2$ and ν_sCH_2 of the adsorbed HCHO (or νCH of the generated formate) (Figure 1c).[6, 9] At 10 ppm HCHO, a weak peak of νC=O at 1788 cm^{-1} emerges (Figure 1g) because of the molecularly adsorbed HCHO.[9] Most of the generated formate is desorbed after two hours re-exposure to air with the evident decreases of the peaks of $\nu_{as}COO^-$ and ν_sCOO^- (Figure 1b, f); there are still some remaining formate species at the surface albeit one has to significantly zoom in to observe them (Figure 1b, lower panel).

Surface oxygen species (lattice oxygen or adsorbed oxygen) are influenced by the HCHO exposure: a pronounced decrease of a band centers around 1000 cm^{-1}, corresponding to the vibration of M-O bond (νInO and νSnO), (Figure 1b, d, g); during recovery (Figure 1f)[8, 9] and under exposure to oxygen in a N_2 background the opposite is observed (Figure S1). In that spectral region, there is a distinctive feature – a small but sharp peak at 1134 cm^{-1} – that can be attributed to the molecular oxygen ion O_2^- ($\nu O_{2\ ads}$).[9, 10] To our knowledge, it is the first experimental observation of that specie, and its involvement in gas sensing, obtained in operando conditions. There is a previous report of its observation at the surface of CeO_2 catalyst with in situ Raman spectroscopy, but at temperatures below 120 °C.[10]

Also the concentration of terminal hydroxyl group (OH_t) changes under HCHO exposure; a clear decrease and increase of νOH_t around 3654 cm^{-1},[6, 8, 9, 11] identified by H_2O-D_2O exchange DRIFTS (Figure S2), are observed when $In_4Sn_3O_{12}$ is exposed to HCHO and re-exposed to air (Figure 1b, c ,e). Because the H_2O-D_2O exchange DRIFTS is measured beforehand, some OD_t groups are still present at the surface during the HCHO exposure measurement. Hence, a decrease at 2690 cm^{-1} (νOD_t) is observed in Figure 1b, c. Despite of the absence of D_2O during the recovery process following the 1.5-ppm-HCHO exposure, interestingly, a small peak at 2696 cm^{-1} (νOD_t) still emerges (Figure 1e). Probably, some D atoms of OD_t are not desorbed but merely migrate to another site and return to OD_t after re-exposure to air.

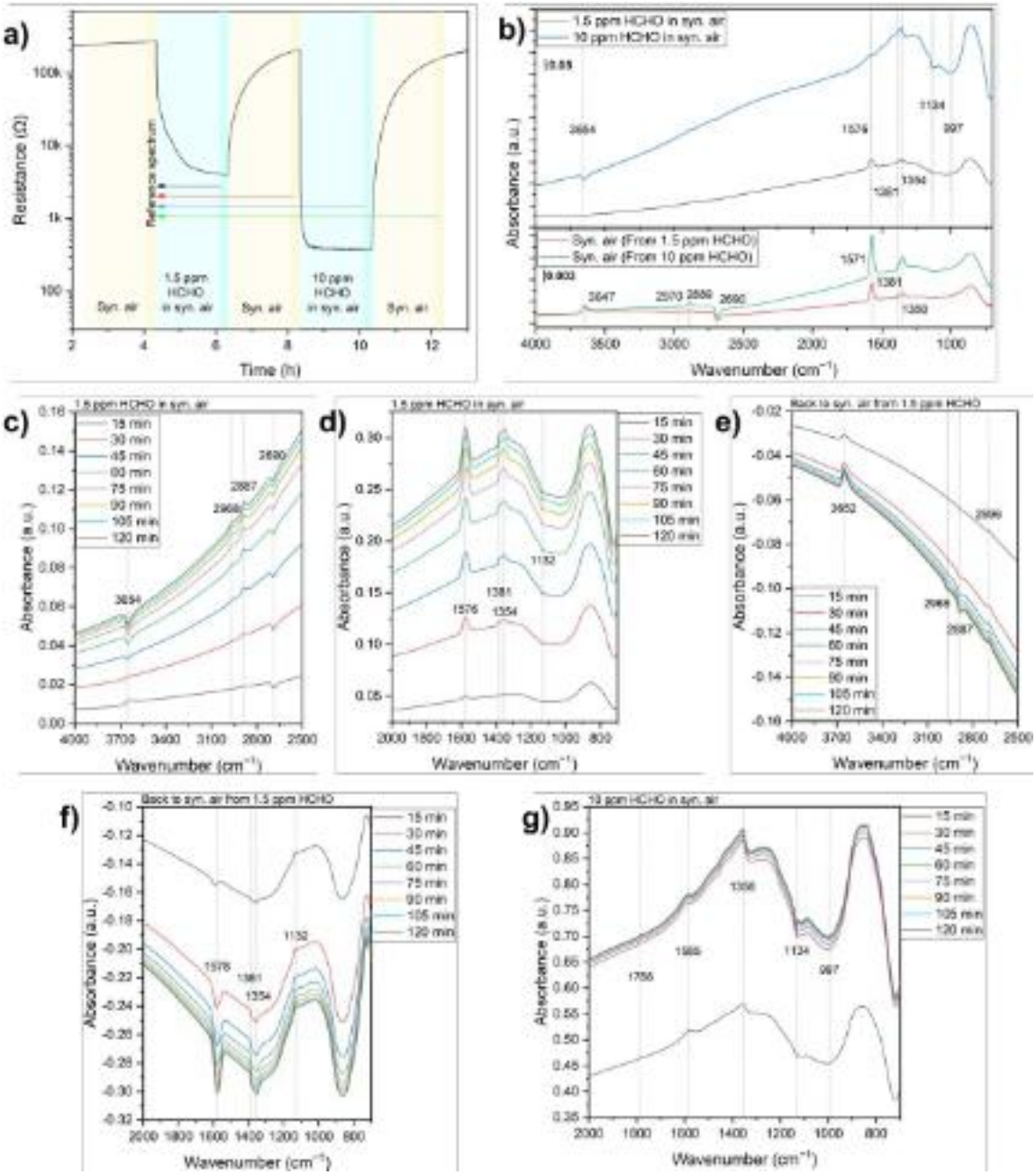

Figure 1 DRIFTS results measured at 200 °C. (a) Resistance curve of the sensor device during HCHO DRIFTS measurement, (b) absorbance spectra calculated by Eq. S1 with the last single channel (SC) in 1.5 ppm HCHO, second-round air, 10 ppm HCHO and third-round air referred to the last SC spectrum in the first-round air exposure (Experimental Details), (c, d) eight absorbance spectra during 2 h exposure to 1.5 ppm HCHO referred to the last SC spectrum in the first-round air exposure, (e, f) eight absorbance spectra during second round air exposure referred to the last SC spectrum in 1.5 ppm HCHO, and (g) eight absorbance spectra during 2 h exposure to 10 ppm HCHO referred to the last spectrum in the second-round air exposure.

The DRIFTS suggests that HCHO is partially oxidized into formate species (or HCOOH) and that no combustion to CO_2 or CO takes place:

- The presence of $-CH_2-$ (2968 and 2887 cm^{-1}) and the absence (or very little in 10 ppm HCHO) of C=O (1788 cm^{-1}) demonstrates the generation of dioxymethylene;[6, 9, 12, 13]
- The generated dioxymethylene is then oxidized into formate;
- Finally, the formate specie desorbs as HCOOH without being further oxidized (Eq. 1, in which the asterisk indicates an adsorbed species);
- Oxygen specie and OH_t take part in the processes.

$$HCHO + O \rightarrow {}^{*}OCH_2O \qquad \text{Eq. 1a}$$

$$^{*}OCH_2O \rightarrow {}^{*}HCOO + {}^{*}H \qquad \text{Eq. 1b}$$

$$^{*}HCOO + {}^{*}H \rightarrow HCOOH \qquad \text{Eq. 1c}$$

The counterintuitive partial oxidation of HCHO arouses several questions: What is the exact role of oxygen species and OH_t? What are the reaction route and corresponding energy profile? How does it result in huge changes in resistance, by Eq. 1a or Eq. 1b?

To answer the questions, we resort to DFT simulation with the focus on oxygen species and OH_t. We performed the simulations on clean stoichiometric $In_4Sn_3O_{12}$ (001) and on $In_4Sn_3O_{12}$ (001) with oxygen vacancies and adsorbed oxygen ($In_4Sn_3O_{12}$ (001)_O_2/V_O) and water related species ($In_4Sn_3O_{12}$ (001)_OH_t).

The examination of various, possible HCHO adsorption sites and the V_O formation energy identify the Sn (3a)-connected O as the active site (Figure S3−5). The, called in the following, active O plays significant roles in both HCHO adsorption and partial oxidation (Figure 2a). The adsorption takes place with the active O catching the C and the surface Sn (18f) bonding to the O (HCHO), making the HCHO spontaneously transform into dioxymethylene with an adsorption energy (E_{ads}) of −1.87 eV (Figure 2a, Movie S1).[6, 9, 12-14] The surrounding metal atoms (Sn and In) of the active oxygen facilities the adsorption; the additional valence electron of Sn, when compared to In, enables Sn-O (HCHO) more energetically favorable (Figure S3−4). For oxidation, another active O, the closest to the dioxymethylene, captures the H atom, generating one formate and one rooted hydroxyl group (OH_{rooted}), with E_a of 0.68 eV (Figure 2a). The whole reaction energy (E_{react}) reaches −3.72 eV. Mulliken charge analysis (Table 1) reveals that sufficient charge transfer (0.440) takes place only after the generation of the formate and the OH_{rooted} (Eq. 1b), and that the OH_{rooted} (actually its H)

makes the main contribution. Additionally, the oxidation process weakens the interaction among the active O and surface metal ions (Figure 2a, right panel 1 and 2), explaining the decrease of νInO and νSnO around 1000 cm^{-1}.

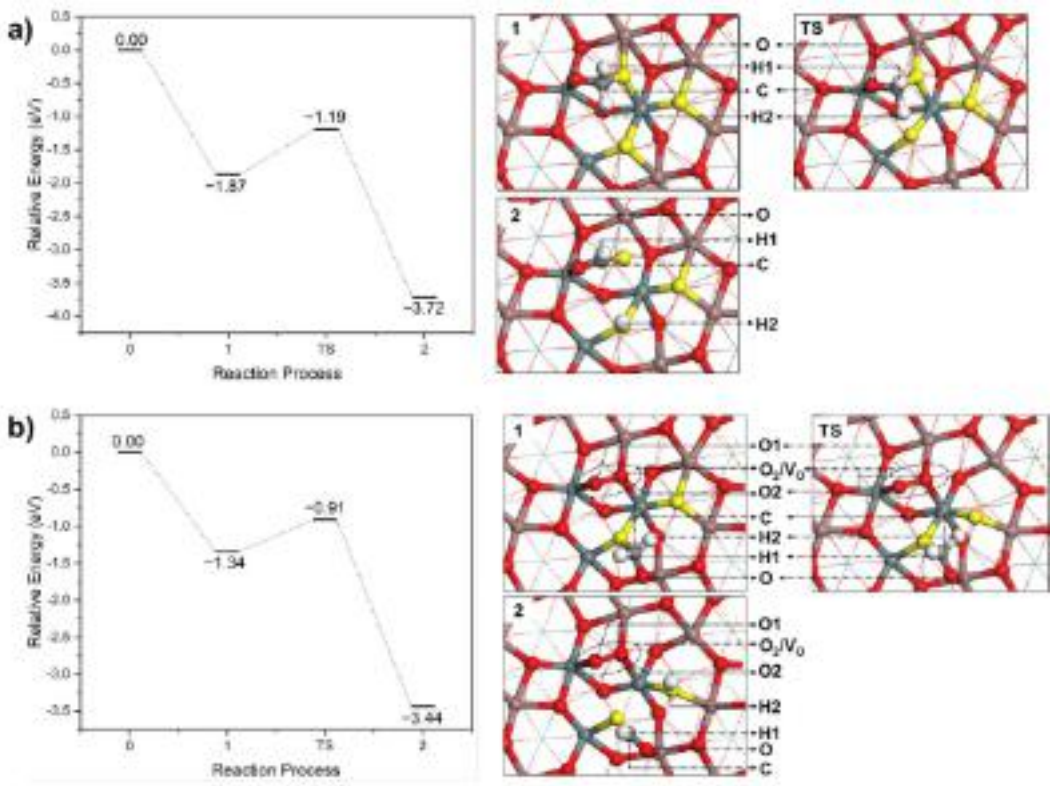

Figure 2 HCHO adsorption and oxidation at: (a) Stoichiometric $In_4Sn_3O_{12}$ (001) and (b) $In_4Sn_3O_{12}$ (001)_O_2/V_O (H, C, O, In, Sn; the bright yellow atom is the active O; TS means transition state.)

Table 1 Mulliken charge analysis of absorbed species at $In_4Sn_3O_{12}$ (001)

Surface	Process	Mulliken charge / *e*							
		HCHO							
		Total	H1	H2	C	O			
$In_4Sn_3O_{12}$ (001)	1	−0.040	0.101	0.105	0.338	−0.584			
	2	0.440	0.095	0.289	0.469	−0.413			
		HCHO					$O_{2\ ads}$		
		Total	H1	H2	C	O	Total	O1	O2
$In_4Sn_3O_{12}$ (001)_O_2/V_O	0						−0.733	−0.337	−0.396
	1	−0.053	0.103	0.106	0.325	−0.587	−0.748	−0.343	−0.405
	2	0.476	0.097	0.289	0.491	−0.401	−0.787	−0.367	−0.420
		HCHO					OH_t		
		Total	H1	H2	C	O	Total	H	O
$In_4Sn_3O_{12}$ (001)_OH_t	0						−0.341	0.284	−0.625
	1	−0.034	0.097	0.117	0.345	−0.593	−0.268	0.357	−0.625
	2	−0.020	0.113	0.107	0.333	−0.573	−0.289	0.332	−0.621
	3	−0.010	0.120	0.115	0.323	−0.568	−0.233	0.296	−0.529
	4	0.366	0.077	0.299	0.438	−0.448	−0.153	0.296	−0.449

Note: The *e* is the elementary electron charge. Positive value represents electron donation effect of adsorbate. The H1, H2 are labeled in Figure 2−3, and the O1, O2 in Figure 2b.

Gaseous O_2 has little interaction with the stoichiometric $In_4Sn_3O_{12}$ (001) but a high tendency to fill the V_O which defect is always present due to the high-temperature synthesis of $In_4Sn_3O_{12}$ (Figure S5−7).[3] Even with O_2/V_O, HCHO still interacts with and then is oxidized by the active O, Sn (3a)-connected, with total E_{react} of −3.34 eV and a little lower E_a of 0.43 eV (Figure 2b, Figure S8), and donates electrons (0.476) to the surface with a few moving to the O_2/V_O (Table 1). Consequently, the O−O bond is elongated from 1.444 to 1.471 Å. The O_2 molecule can dissociate and fill the two V_O, eventually re-generating a stoichiometric surface (Figure S9), once the product (HCOOH) is desorbed to leave the second V_O. This could explain the experimentally observed decrease of the vibration at 1134 cm^{-1} ($\nu O_{2\ ads}$) (Figure 1b, d, g) and gives credence to the hypothesis that the adsorbed molecular oxygen is a precursor for the regeneration of the active O.[15]

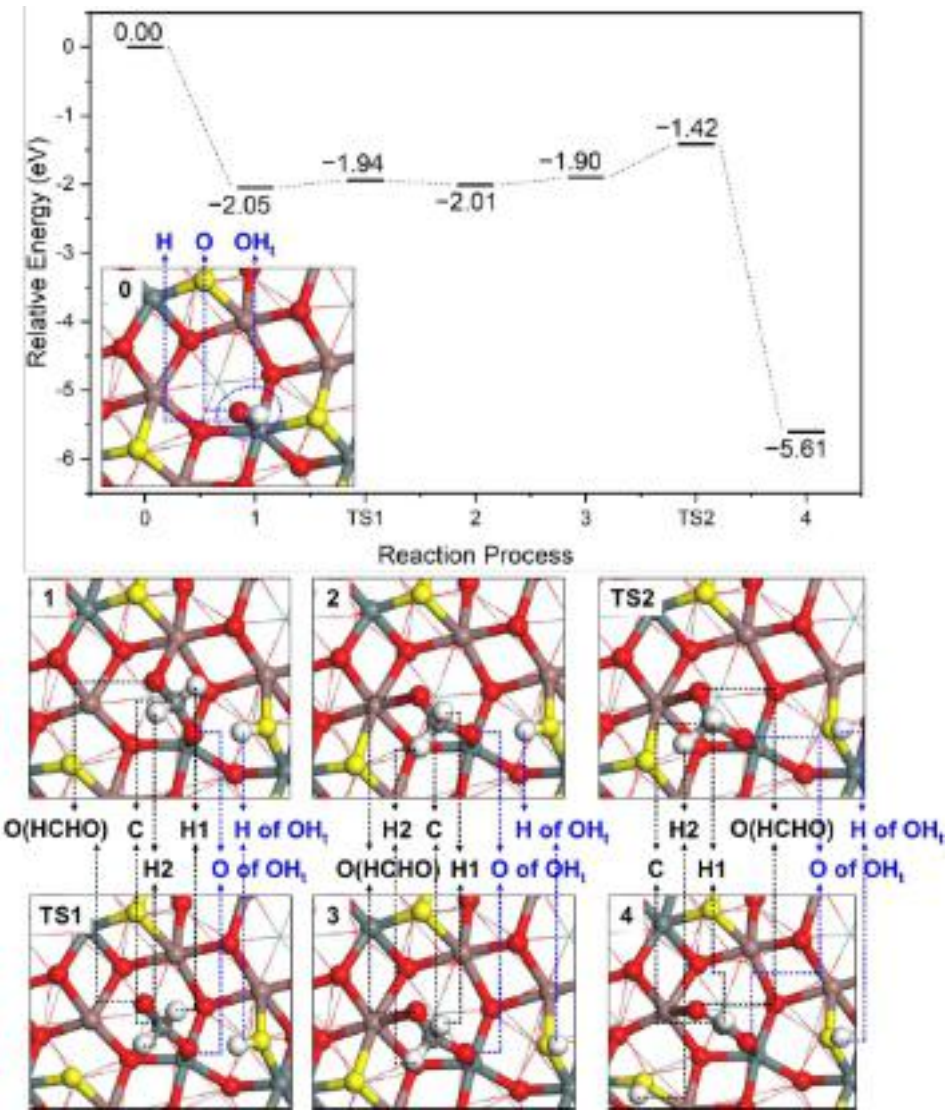

Figure 3 HCHO adsorption and oxidation at $In_4Sn_3O_{12}$ (001)_OH_t

The surface OH_t has already been demonstrated to be able to facilitate the HCHO oxidation.[6, 16, 17] Numerous OH_t is present at the surface, as demonstrated by the H_2O-D_2O exchange DRIFTS (Figure S2), even in dry air (humidity contamination around 100 ppm) at 200 °C. The HCHO prefers to interact with the OH_t to form the dioxymethylene with E_{ads} −2.05 eV (Figure 3, Movie S2), while the active O accepts the H atom from the OH_t to generate an OH_{rooted}. The migration of the H (D) of the OH_t (OD_t) to the OH_{rooted} (OD_{rooted}) provides an opportunity for the re-generation of OH_t (OD_t) by reaction with O_2 molecules in the recovery stage (Eq. 2); this explains the emergence of νOD_t at 2690 cm^{-1} (Figure 1d).

$$2OH_{rooted} + O_2 \rightarrow 2OH_t + 2O_o \qquad \text{Eq. 2a}$$

$$2OD_{rooted} + O_2 \rightarrow 2OD_t + 2O_o \quad \text{Eq. 2b}$$

After the adsorption, the dioxymethylene can swing at the triangle (Sn-In-In) and be oxidized when it is close to another active O with E_a of 0.48 eV (Figure 3). The overall E_{react} is −5.61 eV. The OH_t actually extracts charge (−0.341) from the surface (Table 1), while it gradually gives charge back (−0.153) during HCHO adsorption and partial oxidation. The last step makes the most charge contribution (0.366).

The DRIFTS demonstrates the partial oxidation of HCHO, and the DFT simulation details the reaction route and energy profile as well as the remarkable charge effect of the generated formate and OH_{rooted}. Why in neither the response nor the recovery stage is the formate further oxidized into CO_2 or CO? Theoretical works have revealed that the energy barrier to break the second C−H bond is much higher than to break the first of HCHO.[13, 16] Experiments on HCOOH desorption and decomposition of metal oxides have demonstrated that the formate can hardly decompose into CO and CO_2 at 200 °C.[7, 18] Therefore, the generated formate must be desorbed as HCOOH by taking the H from the OH_{rooted}, leaving behind one V_O which can then be filled by the O_2.

In conclusion, the partial oxidation of HCHO into formate (or HCOOH) is responsible for the sensor signal of $In_4Sn_3O_{12}$ under HCHO exposure at 200 °C. The Sn (3a)-connected O is the active site and plays key roles in both HCHO adsorption and partial oxidation. The presence of OH_t facilitates the HCHO adsorption. The partial oxidation can induce sufficient charge transfer. The E_a for the rate-determining-step of the partial oxidation, i.e. the rupture of the first C−H bond of the dioxymethylene, is in medium range (0.43−0.68 eV), making it feasible at the optimum temperature of 200 °C.

Acknowledgements

We acknowledge the valuable inputs from Anna Staerz and the assistance in experiments from Matthias Boepple, Benjamin Junker and Andre Sackmann. For the computational resources, we are grateful for the support from the Research Centre for Materials Genome Engineering at Wuhan University of Technology, the Shenzhen HUASUAN Technology Company Limited and CALMIP (Grant P16038).

Supporting Information Available

Details of DRIFTS measurement, computational details, building and optimization of $In_4Sn_3O_{12}$ primitive cell and $In_4Sn_3O_{12}$ (001) surface, N_2-O_2 DRIFTS, H_2O-D_2O exchange DRIFTS, and some DFT supporting figures. This material is available free of charge via the internet at http://pubs.acs.org.

References

(1) Yu, C.; Crump, D. A Review of the emission of VOCs from polymeric materials used in buildings. *Building and Environment* **1998**, *33* (6), 357-374. DOI: https://doi.org/10.1016/S0360-1323(97)00055-3. Jones, A. P. Indoor air quality and health. *Atmospheric Environment* **1999**, *33* (28), 4535-4564. DOI: https://doi.org/10.1016/S1352-2310(99)00272-1. Collins, J. J.; Ness, R.; Tyl, R. W.; Krivanek, N.; Esmen, N. A.; Hall, T. A. A Review of Adverse Pregnancy Outcomes and Formaldehyde Exposure in Human and Animal Studies. *Regulatory Toxicology and Pharmacology* **2001**, *34* (1), 17-34. DOI: https://doi.org/10.1006/rtph.2001.1486.

(2) Izawa, K.; Ulmer, H.; Staerz, A.; Weimar, U.; Barsan, N. 5 - Application of SMOX-based sensors. In *Gas Sensors Based on Conducting Metal Oxides*, Barsan, N., Schierbaum, K. Eds.; Elsevier, 2019; pp 217-257. Barsan, N.; Schierbaum, K. *Gas Sensors Based on Conducting Metal Oxides*; Elsevier, 2018. Barsan, N.; Koziej, D.; Weimar, U. Metal oxide-based gas sensor research: How to? *Sensors and Actuators B: Chemical* **2007**, *121* (1), 18-35. DOI: https://doi.org/10.1016/j.snb.2006.09.047. Yamazoe, N. Toward innovations of gas sensor technology. *Sensors and Actuators B: Chemical* **2005**, *108* (1–2), 2-14. DOI: https://doi.org/10.1016/j.snb.2004.12.075.

(3) Kemmler, J. A.; Pokhrel, S.; Birkenstock, J.; Schowalter, M.; Rosenauer, A.; Bârsan, N.; Weimar, U.; Mädler, L. Quenched, nanocrystalline In4Sn3O12 high temperature phase for gas sensing applications. *Sensors and Actuators B: Chemical* **2012**, *161* (1), 740-747. DOI: https://doi.org/10.1016/j.snb.2011.11.026.

(4) Chu, X.; Chen, T.; Zhang, W.; Zheng, B.; Shui, H. Investigation on formaldehyde gas sensor with ZnO thick film prepared through microwave heating method. *Sensors and Actuators B: Chemical* **2009**, *142* (1), 49-54. DOI: https://doi.org/10.1016/j.snb.2009.07.049. Park, H. J.; Choi, N.-J.; Kang, H.; Jung, M. Y.; Park, J. W.; Park, K. H.; Lee, D.-S. A ppb-level formaldehyde gas sensor based on CuO nanocubes prepared using a polyol process. *Sensors and Actuators B: Chemical* **2014**, *203*, 282-288. DOI: https://doi.org/10.1016/j.snb.2014.06.118. Li, Y.; Chen, N.; Deng, D.; Xing, X.; Xiao, X.; Wang, Y. Formaldehyde detection: SnO2 microspheres for formaldehyde gas sensor with high sensitivity, fast response/recovery and good selectivity. *Sensors and Actuators B: Chemical* **2017**, *238*, 264-273. DOI: https://doi.org/10.1016/j.snb.2016.07.051. Xu, R.; Zhang, L.-X.; Li, M.-W.; Yin, Y.-Y.; Yin, J.; Zhu, M.-Y.; Chen, J.-J.; Wang, Y.; Bie, L.-J. Ultrathin SnO2 nanosheets with dominant high-energy {001} facets for low

temperature formaldehyde gas sensor. *Sensors and Actuators B: Chemical* **2019**, *289*, 186-194. DOI: https://doi.org/10.1016/j.snb.2019.03.012.

(5) Xu, J.; White, T.; Li, P.; He, C.; Han, Y.-F. Hydroxyapatite Foam as a Catalyst for Formaldehyde Combustion at Room Temperature. *Journal of the American Chemical Society* **2010**, *132* (38), 13172-13173. DOI: 10.1021/ja1058923.

(6) Zhang, C.; Liu, F.; Zhai, Y.; Ariga, H.; Yi, N.; Liu, Y.; Asakura, K.; Flytzani-Stephanopoulos, M.; He, H. Alkali-Metal-Promoted Pt/TiO2 Opens a More Efficient Pathway to Formaldehyde Oxidation at Ambient Temperatures. *Angewandte Chemie International Edition* **2012**, *51* (38), 9628-9632. DOI: https://doi.org/10.1002/anie.201202034. Li, Y.; Chen, X.; Wang, C.; Zhang, C.; He, H. Sodium Enhances Ir/TiO2 Activity for Catalytic Oxidation of Formaldehyde at Ambient Temperature. *ACS Catalysis* **2018**, *8* (12), 11377-11385. DOI: 10.1021/acscatal.8b03026. Chen, X.; He, G.; Li, Y.; Chen, M.; Qin, X.; Zhang, C.; He, H. Identification of a Facile Pathway for Dioxymethylene Conversion to Formate Catalyzed by Surface Hydroxyl on TiO2-Based Catalyst. *ACS Catalysis* **2020**, *10* (17), 9706-9715. DOI: 10.1021/acscatal.0c01901.

(7) Fein, D. E.; Wachs, I. E. Quantitative Determination of the Catalytic Activity of Bulk Metal Oxides for Formic Acid Oxidation. *Journal of Catalysis* **2002**, *210* (2), 241-254. DOI: https://doi.org/10.1006/jcat.2002.3683.

(8) Wicker, S.; Guiltat, M.; Weimar, U.; Hémeryck, A.; Barsan, N. Ambient Humidity Influence on CO Detection with SnO2 Gas Sensing Materials. A Combined DRIFTS/DFT Investigation. *The Journal of Physical Chemistry C* **2017**, *121* (45), 25064-25073. DOI: 10.1021/acs.jpcc.7b06253.

(9) Davydov, A. Molecular Spectroscopy of Oxide Catalyst Surfaces. **2003**.

(10) Schilling, C.; Ganduglia-Pirovano, M. V.; Hess, C. Experimental and Theoretical Study on the Nature of Adsorbed Oxygen Species on Shaped Ceria Nanoparticles. *The Journal of Physical Chemistry Letters* **2018**, *9* (22), 6593-6598. DOI: 10.1021/acs.jpclett.8b02728.

(11) Boehme, I.; Weimar, U.; Barsan, N. Unraveling the Surface Chemistry of CO Sensing with In2O3 Based Gas Sensors. *Sensors and Actuators B: Chemical* **2021**, *326*, 129004. DOI: https://doi.org/10.1016/j.snb.2020.129004. Degler, D.; Junker, B.; Allmendinger, F.; Weimar, U.; Barsan, N. Investigations on the Temperature-Dependent Interaction of Water Vapor with Tin Dioxide and Its Implications on Gas Sensing. *ACS Sensors* **2020**, *5* (10), 3207-3216. DOI: 10.1021/acssensors.0c01493.

(12) Zhou, J.; Mullins, D. R. Adsorption and reaction of formaldehyde on thin-film cerium oxide. *Surface Science* **2006**, *600* (7), 1540-1546. DOI: https://doi.org/10.1016/j.susc.2006.02.009.

(13) Teng, B.-T.; Jiang, S.-Y.; Yang, Z.-X.; Luo, M.-F.; Lan, Y.-Z. A density functional theory study of formaldehyde adsorption and oxidation on CeO2(111) surface. *Surface Science* **2010**, *604* (1), 68-78. DOI: https://doi.org/10.1016/j.susc.2009.10.024.

(14) Busca, G.; Lamotte, J.; Lavalley, J. C.; Lorenzelli, V. FT-IR study of the adsorption and transformation of formaldehyde on oxide surfaces. *Journal of the American Chemical Society* **1987**, *109* (17), 5197-5202. DOI: 10.1021/ja00251a025.

(15) Gurlo, A. Interplay between O2 and SnO2: Oxygen Ionosorption and Spectroscopic Evidence for Adsorbed Oxygen. *ChemPhysChem* **2006**, *7* (10), 2041-2052. DOI: https://doi.org/10.1002/cphc.200600292. Yang, T.; Liu, Y.; Jin, W.; Han, Y.; Yang, S.; Chen, W. Investigation on the Transformation of Absorbed Oxygen at ZnO $\{10\bar{1}0\}$ Surface Based on a Novel Thermal Pulse Method and Density Functional Theory Simulation. *ACS Sensors* **2017**, *2* (7), 1051-1059. DOI: 10.1021/acssensors.7b00363. Yuan, H.; Aljneibi, S. A. A. A.; Yuan, J.; Wang, Y.; Liu, H.; Fang, J.; Tang, C.; Yan, X.; Cai, H.; Gu, Y.; et al. ZnO Nanosheets Abundant in Oxygen Vacancies Derived from Metal-Organic Frameworks for ppb-Level Gas Sensing. *Advanced Materials* **2019**, *31* (11), 1807161. DOI: https://doi.org/10.1002/adma.201807161. Kim, K.; Choi, P. g.; Itoh, T.; Masuda, Y. Catalyst-free Highly Sensitive SnO2 Nanosheet Gas Sensors for Parts per Billion-Level Detection of Acetone. *ACS Applied Materials & Interfaces* **2020**, *12* (46), 51637-51644. DOI: 10.1021/acsami.0c15273.

(16) Wang, X.; Rui, Z.; Ji, H. DFT study of formaldehyde oxidation on silver cluster by active oxygen and hydroxyl groups: Mechanism comparison and synergistic effect. *Catalysis Today* **2020**, *347*, 124-133. DOI: https://doi.org/10.1016/j.cattod.2018.06.021.

(17) Bai, B.; Li, J. Positive Effects of K+ Ions on Three-Dimensional Mesoporous Ag/Co3O4 Catalyst for HCHO Oxidation. *ACS Catalysis* **2014**, *4* (8), 2753-2762. DOI: 10.1021/cs5006663.

(18) Durand, J. P.; Senanayake, S. D.; Suib, S. L.; Mullins, D. R. Reaction of Formic Acid over Amorphous Manganese Oxide Catalytic Systems: An In Situ Study. *The Journal of Physical Chemistry C* **2010**, *114* (47), 20000-20006. DOI: 10.1021/jp104629j.

TOC graphic

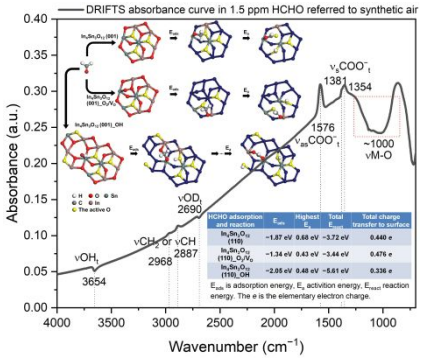
DRIFTS absorbance curve in 1.5 ppm HCHO referred to synthetic air
Absorbance (a.u.)
Wavenumber (cm^{-1})
0.00
0.05
0.10
0.15
0.20
0.25
0.30
0.35
0.40
4000
3500
3000
2500
2000
1500
1000
νOH$_t$
3654
νCH$_2$ or νCH
2968
2887
νOD$_t$
2690
1576
ν_{as}COO^-_t
ν_sCOO^-_t
1381
1354
~1000
νM-O
C H
O Sn
C In
The active O
HCHO adsorption and reaction
E_{ads}
Highest E_a
Total E_{react}
Total charge transfer to surface
$In_2Sn_2O_{12}$ (110)
−1.87 eV
0.68 eV
−3.72 eV
0.440 e
$In_2Sn_2O_{12}$ (110)_O_t/V_o
−1.34 eV
0.43 eV
−3.44 eV
0.476 e
$In_2Sn_2O_{12}$ (110)_OH
−2.05 eV
0.48 eV
−5.61 eV
0.336 e
E_{ads} is adsorption energy, E_a activition energy, E_{react} reaction energy. The e is the elementary electron charge.